Evaluation of Parameters Used in Progressive Damage Models

September 2022

Final report

U.S. Department of Transportation
Federal Aviation Administration

NOTICE

This document is disseminated under the sponsorship of the U.S. Department of Transportation in the interest of information exchange. The U.S. Government assumes no liability for the contents or use thereof. The U.S. Government does not endorse products or manufacturers. Trade or manufacturers' names appear herein solely because they are considered essential to the objective of this report. The findings and conclusions in this report are those of the author(s) and do not necessarily represent the views of the funding agency. This document does not constitute FAA policy. Consult the FAA sponsoring organization listed on the Technical Documentation page as to its use.

This report is available at the Federal Aviation Administration William J. Hughes Technical Center's Full-Text Technical Reports page: actlibrary.tc.faa.gov in Adobe Acrobat portable document format (PDF).

Form DOT F 1700.7 (8-72) Reproduction of completed page authorized

1. Report No. DOT/FAA/TC-22/8	2. Government Accession No.	3. Recipient's Catalog No.
4. Title and Subtitle Evaluation of Parameters Used in Progressive Damage Models		5. Report Date September 2022
		6. Performing Organization Code ANG-E281
7. Author(s) D. Plechaty, S. Solanki, T. Moore, J. P. Parmigiani		8. Performing Organization Report No.
9. Performing Organization Name and Address School of MIME Oregon State University Corvallis, OR 97331		10. Work Unit No. (TRAIS)
		11. Contract or Grant No.
12. Sponsoring Agency Name and Address Policy & Innovation Division AIR-600 Aviation Safety, FAA Seattle Headquarters 2200 S 216th St, Des Moines, WA 98198-6547		13. Type of Report and Period Covered
		14. Sponsoring Agency Code AIR-600
15. Supplementary Notes The Federal Aviation Administration William J. Hughes Technical Center Research Division, COR was Lynn Pham.		

16. Abstract

Damage initiation and propagation in carbon fiber composites can be classified as corresponding to loading of the fibers in tension & compression, the matrix in tension & compression, and the matrix in shear. Matrix compression has been studied the least. The matrix-compression damage parameters needed for finite element simulations are not available. Matrix-tension values are typically used. While such estimates are sufficiently conservative (i.e., result in predictions of failure at lower loads than would occur and are thus "safe") the difference from the correct matrix-compression values are unknown. Consequently, this approach may lead to overly conservative designs. The purpose of this project is to evaluate currently-used finite element methods to determine the extent to which the use of these incorrect matrix-compression damage parameters impacts simulation predictions and calculations. The method used was to determine accurate matrix-compression damage parameters, use them in simulations, and compare the outputs to those obtained from the current approach of using tensile values. Accurate matrix-compression damage parameters were determined through development of a suitable test specimen and experimental measurements. With these parameters simulations for several layups and loadings were performed with the commercial finite element package and compared to simulations using tensile values. Results showed that the appropriate matrix-compression damage material model was an energy release rate at the propagating tip of the damage region. The contribution of residual load-carrying ability in the wake of this tip (due to surface contact under compressive loading) was insignificant. Furthermore, the energy release rate was found to consist of Mode I and Mode II components of respective magnitudes of 3.42 times the currently-used tensile value and 11.88 times the currently-used tensile value. The extent to which the use of incorrect matrix-compression damage parameters impacts simulation predictions and calculations was evaluated using six layups and two loading configurations. Results showed the change in value did not significantly affect fiber-tension damage or fiber-compression damage for any layup or loading and only slightly affected Mises stress. However, the change in value did significantly affect matrix-tension damage, matrix-compression damage, and matrix-shear damage for all layups and both loadings. This report shows that the current method using a tensile value for matrix-compression damage can introduce significant errors in predictions of damage initiation and propagation in finite element simulations of carbon-fiber laminates.

| 17. Key Words

1.   Carbon Fiber – Finite Element Analysis
2.   Carbon Fiber – Matrix Compression
3.   Carbon Fiber – Damage Initiation
4.   Carbon Fiber – Damage Propagation
5.   Carbon Fiber – Fracture Toughness | 18. Distribution Statement

This document is available to the U.S. public through the National Technical Information Service (NTIS), Springfield, Virginia 22161. This document is also available from the Federal Aviation Administration William J. Hughes Technical Center at actlibrary.tc.faa.gov. | | |
| 19. Security Classif. (of this report)
Unclassified | 20. Security Classif. (of this page)
Unclassified | 21. No. of Pages
44 | 19. Security Classif. (of this report)
Unclassified |

Contents

Figures

Tables

Acronyms

Acronym	Definition
FAA	Federal Aviation Administration
FEA	Finite Element Analysis
SCC	Stepped Compact Compression
LEFM	Linear Elastic Fracture Mechanics
AMTAS	The Center of Excellence for Advanced Materials in Transport Aircraft Structures

Executive summary

Efficient and effective design for aerospace carbon-fiber components depends on accurate modeling to predict performance. Often this modeling consists of finite element simulations of damage initiation and propagation. Damage initiation and propagation in carbon fiber composites can be classified as corresponding to loading of the fibers in tension, the fibers in compression, the matrix in tension, the matrix in compression, or the matrix in shear. Of these, damage initiation and propagation corresponding to matrix compression has been studied the least. This lack of study results in the unavailability of needed matrix-compression damage parameters for finite element simulations. In response, matrix-tension values are typically used as estimates. While it is highly likely that such estimates are sufficiently conservative (i.e., result in predictions of failure at lower loadings than would actually occur and are thus "safe") the specific magnitude of the difference from the actual matrix-compression values are unknown. Consequently, this approach may lead to overly conservative designs.

The purpose of this project is to evaluate current finite element methods to determine the extent to which the use of incorrect matrix-compression damage parameters impacts simulation predictions and calculations. The method used was to determine accurate matrix-compression damage parameters, use them in simulations, and compare the outputs to those obtained from the current approach using tensile values. Accurate matrix-compression damage parameters were determined through development of a suitable test specimen and experimental measurements. These measurements were used to develop an accurate matrix-compression damage material model and calculate the parameters needed for finite element modeling. With these values, simulations for several layups and loadings were performed with the commercial finite element package ABAQUS using the matrix-compression parameters obtained in this study and the matrix-compression parameters currently used (i.e., matrix-tension values).

Results showed that the appropriate matrix-compression damage material model was an energy release rate at the propagating tip of the damage region. The contribution of residual load-carrying ability in the wake of this tip, due to surface contact under compressive loading, was insignificant. Furthermore, through an experimentally-observed phase angle of approximately 62 degrees this energy release rate was found to consist of Mode I and Mode II components of respective magnitudes of 3.42 times the currently used value and 11.88 times the currently used value. Combined, the total matrix-compression energy release rate determined through this study was 15.3 times the currently used value. Experimental variation was relatively high with standard deviation values of 6.01 times the currently used value for total energy release rate, 1.72

times the currently-used value for Mode I energy release rate, 4.69 times the currently-used value for Mode II energy release rate, and 4.16 degrees for phase angle.

As a validation of the test specimen and test approach, the matrix-tension energy release rate was determined using the same specimen (but loaded in tension), materials, test equipment, and analysis methods as used for matrix-compression. The result was a mean value of the matrix-tension energy release rate of 1.16 times the currently used value with a standard deviation of 0.39 times the currently used value. Since this value falls within the experimental uncertainty of the measurement the method is considered validated.

The extent to which the use of incorrect matrix-compression damage parameters impacts simulation predictions and calculations was evaluated using six layups and two loading configurations. All input properties were the same except the matrix-compression damage parameter, which was assumed to be equal to the matrix-tension parameter or consistent with matrix-compression test results from this study. Specifically, notched laminates having 40 plies with 10%, 30%, and 50% zero degree plies, and 20 plies with 10%, 30%, and 50% zero-degree plies were loaded by out-of-plane shear and out-of-plane bending. Comparisons of Mises stress, fiber-tension and fiber-compression damage, and matrix-tension and matrix-compression damage, were made using the currently used manufacturer's value (i.e., tensile value) and the value determined in this study. Results showed the change in value did not significantly affect fiber-tension damage or fiber-compression damage for any layup or loading and only slightly affected Mises stress. However, the change in value did significantly affect matrix-tension damage, matrix-compression damage, and matrix-shear damage for all layups and both loadings.

This report shows that the current method of simply using a tensile value for matrix-compression damage can introduce significant errors in predictions of damage initiation and propagation in finite element simulations of carbon fiber laminates.

1   Technical basis

A significant motivation to better understand the damage initiation and propagation behavior in composite materials is their increased use in aircraft structures. Composite materials can often carry increased load during damage accumulation before ultimate failure. Therefore, the damage propagation behavior of a composite material is important in determining the failure behavior. The two materials (fiber and matrix) having dissimilar mechanical behavior interacting in composites requires knowledge on the mechanical behavior of each material individually to fully classify the composite behavior. In addition, there are several different failure modes in composites due to differences in the component materials. The major damage propagation modes associated with fiber composites are the fiber in tension and compression and the matrix in tension, compression, and shear. There is extensive literature on fiber tension (Jose, Kumar, Jana, & Rao, 2001; Toygar, Toparly, & Uyulgan, 2006.; Kongshavn & Poursartip, 1999; Laffan, Pinho, Robinson, & Iannucci, 2010; Laffan, Pinho, Robinson, & McMillan, 2011; Gutkin, Laffan, Pinho, Robinson, & Curtis, 2011), matrix tension (Han, Hahn, & Croman, 1988; Maimi P. , Camanho, Mayugo, & Turon, 2011) and fiber compression (Jelf & Fleck, 1992; Sutcliffe & Fleck, 1994; Pinho, Gutkin, Pimenta, De Carvalho, & Robinson, 2012; Gutkin, Pinho , Robinson, & Curtis, 2010). Little research has directly addressed matrix-compression failure. However, significant published research does exist for other failure modes which includes matrix compression as a contributing factor. This body of literature will be considered next.

Fiber micro-buckling is a common compressive damage mechanism studied in literature. Fiber micro-buckling is a failure mode where instabilities cause the fiber to buckle giving the appearance of a wave in the failed material. Researchers note that the matrix properties partially govern this behavior. Four studies relating fiber micro-buckling with matrix-compression damage propagation are discussed in chronological order. Jelf and Fleck (1992) reviewed compressive damage modes on composites using literature, micromechanics model materials, and a case study of PEEK/carbon fiber compressive failure. The researchers determined plastic micro-buckling is the most common failure mode in polymeric composites. In addition, they noted that the matrix shear properties are important for the micro-buckling damage mode. This conclusion is built upon work by Budiansky (1983) and Argon (1972). Fleck et al. (1995) determined micro-buckling was the main failure mechanism for compressive loading tests of notched and unnotched specimens. The specimen layups and materials considered included $[(\pm45/0_2)_3]_s$ layups for an epoxy based and a thermoplastic based material, $[(0/90)_3]$ woven composite specimens, 3-D woven specimens, 0° Beechwood samples, and [0/90/0/90/0] birch plywood. The researchers presented a model for the fracture energy of orthotropic materials.

This model assumes that the energy value includes dissipation from fiber buckling, matrix plasticity, and delamination. The latter two are dominated by matrix properties. Narayanan and Schadler (1999) concluded composites loaded in compression form damage-zones causing matrix-shear instabilities which propagate kink bands. The specimens used in the experimental portion of the study were four point bending specimens with all fibers in the direction of the internal loads. This conclusion suggests that damage propagation is partially governed by the shear properties of the matrix and illustrates that the fiber micro-buckling failure mode is partially governed by the matrix behavior under compression. Soutis and Curtis (2000) present a method for calculating the fracture toughness of a composite undergoing fiber micro-buckling using critical crack closing displacement and unnotched strength of the panel. The nonlinear shear properties of the matrix are incorporated in this model. Vinod et al. (2010), used fractography to identify the main failure modes of carbon fiber under compression loading. The major fracture mode identified was fiber of kinking and kink band propagation. The researchers note that the strength in compression is limited by the ability of the matrix to support the fibers.

Often simplifying assumptions are made about the behavior of the matrix. Pinho et al (2006), assumed matrix compressive energy release rate can be approximated as the Mode II fracture toughness of the matrix (Argon, 1972). They assumed that the matrix failure can be represented as a single Mode II crack in the 90° layers. A crack in the 90° layers is considered because these layers isolate the matrix properties as the loading is perpendicular to the fiber direction. Based on the work of Puck and Schurmann (1998), it is assumed that the energy dissipation can be calculated from the shear-energy release rate and the angle of the fracture. A fracture plane angle of 53 degrees through the thickness of the plies is often used in this model. Soutis and Curtis (2000) used similar assumptions to separate the fiber-toughness from the matrix-toughness values. This assumption also provides a simplified model for the propagation of compressive damage in the matrix. The calculated strain-energy release rates are implemented into continuum damage mechanics numerical models. Continuum-damage mechanics use a thermodynamics-based approach to degrade the stiffness of a material by the energy dissipated by the damaged region. These models are outlined for composite laminates by Lapczyk and Hurtado (2007) and Maimi et al (2007), with the former being implemented in the Finite Element Analysis (FEA) program ABAQUS. Both models use the crack band theory (Bazant & Oh, 1983) to reduce the mesh dependency of the energy dissipation.

Matrices in composites are most commonly polymer materials. Therefore, it is useful to understand the compressive damage behavior of an unreinforced polymer. Lu et al (1995) applied a hysteresis method to calculate the J-integral for the Mode I fracture toughness of a

polymer. The researchers noted the J-integral technique shows promise for polymeric materials that linear elastic fracture mechanics (LEFM) fails to predict accurately.

Researchers have proposed several criteria for the compressive strength of matrices in a composite that illustrate different assumptions and roles the matrix plays in composite damage. Davila et al (2005) proposed a strength-based failure criteria for matrix compression derived from the Mohr-Coulomb criterion and the angle of the fracture plane. Gonzalez and Llorca (2007) determined that shear bands are the dominant mechanisms of failure in the matrix. Shear bands are narrow regions of extreme shear strain (usually plastic) in the composite matrix. They assumed the matrix behaves as an isotropic, thermo-elasto-plastic solid. Their model includes the plastic deformation of the matrix. These criteria further illustrate matrix properties that govern failure mechanisms of the matrix under compression.

In finite element simulations, current practice often assumes matrix-compression damage initiation and propagation behavior and properties are the same as those for matrix tension. Greatly simplifying, this approach can lead to inaccurate predictions that are at best overly conservative. There is a need for improved analysis techniques and an accurate material model and corresponding properties for matrix-compression failure. The work presented in this report contributes to meeting this need.

This report covers work done under the Advanced Materials in Transport Aircraft Structures (AMTAS) project "Evaluation of Parameters used in Progressive Damage Models", which has some relationship with the end of a previous project that designed the test specimen (see Section 2.1). This part of the work deals with the study of matrix-compression damage in notched carbon fiber laminate panels. Specifically, the creation, manufacture, and use of an experimental test specimen to identify and quantify matrix-compression behavior and the implementation of the resulting material model into finite element simulations to evaluate its effect. The remainder of this report describes this creation, manufacture, use, and modeling.

2   Specimen design and manufacturing

2.1   Design

The design of the test specimen for this project was conducted as part of the AMTAS project: *Failure of Notched Laminates Under Out-of-Plane Bending*. This work is described in the 2019 Federal Aviation Administration (FAA) report "Research Studies for Notched Laminates Under Out-of-Plane Bending" (DOT/FAA/TC-20/7). It describes the use of experimentation and the finite element analysis program ABAQUS, which resulted in the design of a test specimen,

referred to as the *Stepped Compact Compression Specimen* (SCC) for the study of matrix-compression damage (Daniels & Rawlings, 2016; Daniels, Rawlings, & Parmigiani, 2017; Rawlings, Carpenter, & Parmigiani, 2018; McKinley, Carpenter, & Parmigiani, 2018).

The SCC specimen is illustrated below in Figure 1. It consists of a 15-ply thin region around the notch tip and 35-plies elsewhere. All laminate fibers in the specimen are oriented at 90° (i.e., parallel to the notch). Loading is applied at the two 12.70 mm diameter circular holes via pins connected to a mechanical testing machine. The loading at each circular hole is collinear with the other circular hole and directed towards it thus causing compression at the notch tip. Matrix-compression damage initiates at the notch tip and propagates approximately collinear with the notch through the thin region. Tensile failure at the edge of the specimen opposite the notch typically terminates a test by completely fracturing the specimen into two pieces.
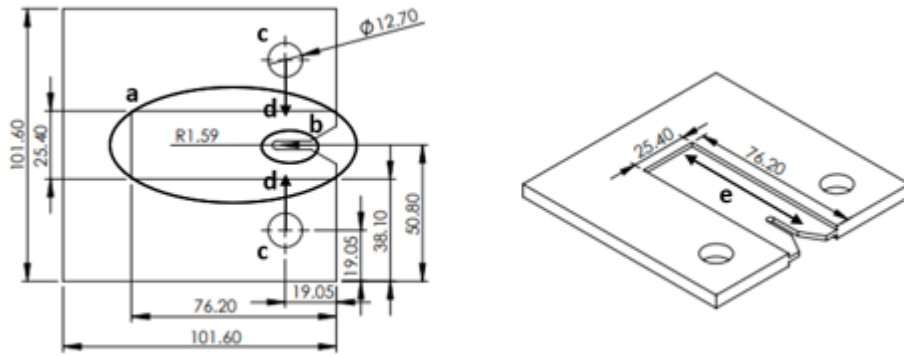
Figure 1. Stepped compact compression specimen showing (a) thin region where matrix-compression damage occurs, (b) notch where matrix-compression damage initiates, (c) locations where loading is applied, (d) direction of the applied loading, and (e) laminate fiber oriented at 90°, parallel to the notch. Dimensions are in mm

2.2 Manufacturing

Effective and efficient manufacturing methods for this specimen were developed through this project. Specifically, these methods consisted of ply geometry, layup method, and procedure, curing and cutting of test specimens.

2.2.1 Ply geometry

Ply geometry for mass manufacturing consisted of 35 90° carbon fiber plies (20 slotted, 15 rectangular) illustrated in Figure 2. The ply geometries allowed up to ten specimens made per layup set.
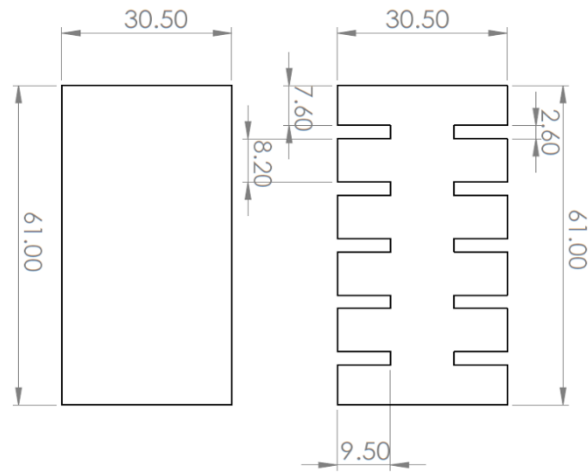
Figure 2. Slotted ply geometry (right) and the rectangular ply geometry (left). Dimensions are in cm.

2.2.2 Layup method

The layup manufacturing method, referred to as the Floating Shim method, is shown in Figure 3. The method uses a flat aluminum plate, a caul plate, 35 90° carbon fiber plies (20 slotted, 15 rectangular) cut using a ply cutter, and 20 rectangular metal shims (two needed per specimen). The shims in this method are placed on the bottom of the aluminum plate and on the top of the carbon fiber to produce the mold. The shims on both sides of the carbon fiber allow the material to move during the cure cycle to reduce damages that could occur from the mold.

Figure 3. Floating shim manufacturing method layup system.

2.2.3 Layup procedure

Ply layup was performed as follows. First, each metal component was coated in Fibre Glast #1153 FibRelease to help the carbon fiber mold separation process. Next, a single slotted ply was placed on the top of the flat aluminum plate. Once placed, the carbon fiber was pressed down with a smooth wedge to take out any possible air bubbles between the carbon fiber and the aluminum plate. Then, the paper attached to the carbon fiber was removed and a razor was moved parallel to the fibers to slit any excess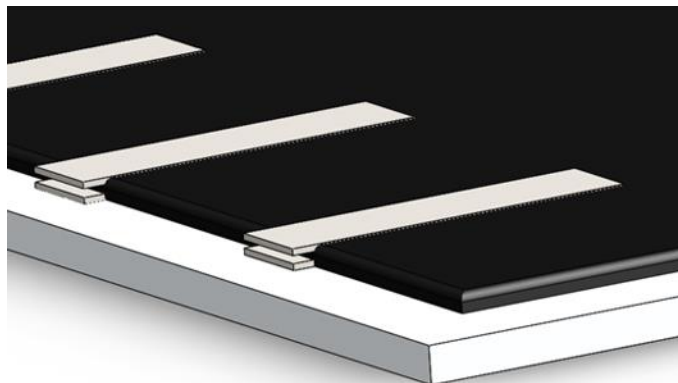 air bubbles formed. After the paper was removed, the next slotted ply was placed directly on the other, with any air bubbles removed by smoothing and slitting the material. This process was repeated for ten of the slotted plies. The 15 rectangular plies were placed upon each other, following the same manufacturing methods. After the rectangular plies were placed, the rectangular shims were placed directly in line with the shims associated with the bottom slotted plies. Once in line, a single slotted ply was placed to fit in between the floating shims on the top rectangular ply and pressed to the preexisting carbon fiber. The nine remaining slotted plies were placed upon each other to complete the layup procedure.

Once the layup procedure was completed, the material was bagged for curing, following typical vacuum molding procedures outlined in the manufacturing processes of Gay (2014) and included a caul plate. The caul plate was placed on top of the carbon fiber to apply extra pressure on the material to reduce delaminations between the plies.

2.2.4 Curing

Upon completion of ply layup and bagging, the material was cured according to the suppliers' specifications and recommendations.

2.2.5 Cutting

All specimens were cut using a ply cutter with a roller blade attachment. The 20 slotted plies were cut to 61 x 30.5 cm and have five 2.6 x 9.5 cm slots along the long edge. The 15 rectangular plies were cut to 61 x 30.5 cm dimensions.

2.2.6 Outcome

These manufacturing methods resulted in a usable specimen success rate ranging between 63% and 88%. Specimens identified as unusable possessed at least one of two manufacturing defects. These include (1) specimen damage along the edges of the thin region as identified in Figure 4 or (2) delamination between ply layers as identified in Figure 5. The first defect was caused by the constriction of material movement during the curing cycle. Using the Floating Shim Method allowed the material to thermally expand and move during curing and thus reduce thermal stress

concentration along the edge of the thin region. The second defect was caused by a lack of applied pressure on the material during curing. Carefully following the material manufacturer's instructions of autoclave curing significantly reduced this defect.

Figure 4. Damages along the thin regions of the cured carbon fiber plate.

Figure 5. Delaminations on the SCC specimen.

3   Testing procedures

All tests were conducted on an ADMET eXpert 2653 lead screw driven universal testing machine using a 45 kN load cell with a resolution of 0.44 N. Displacement measurements were taken from the crosshead of the testing machine. Testing methods were written within ADMET's MTEST Quattro software before tests were conducted. Prior to testing, specimens were installed into the testing machine by placing the loading pins though two clevis fixtures and the specimen. Once placed, two Point Grey Flir Grasshopper GRAS-50S5M-C cameras were focused on the specimen surface to collect images for crack measurements. Using a Labview Vi images were taken at 7.5 frames per second (fps) during testing. The testing procedure consisted of:

1. Loading the specimen until damage initiation occurs (typically at a load of greater than 20 lb.). Damage initiation is visible as a crack which instantaneously appears at the specimen's notch tip and parallel to the notch.
2. Unloading back to 0.008 in. of displacement.
3. Reloading specimen until damage propagation occurs (approximately 0.005 in. of displacement of additional displacement beyond the displacement at which damage initiation occurred). Damage propagation is visible as an extension of the existing crack emanating from the specimen's notch tip.
4. Repeat steps 2 and 3 (unload-reload) until tensile failure occurs on the back edge of the specimen.

4   Analysis methods

A load-displacement curve of a typical test is shown in Figure 6. Following testing images were taken of the notch tip to determine the fracture surface width and load displacement data was written to a csv file.

Load-Displacement Curve of Test Procedure

Legend:
- Damage Initiation Loading
- Damage Initiation Unloading
- Propagation 1 Loading
- Propagation 1 Unoading
- Propagation 2 Loading
- Propagation 2 Unoading
- Tensile Failure Back Edge Loading
- Tensile Failure Back Edge Unloading
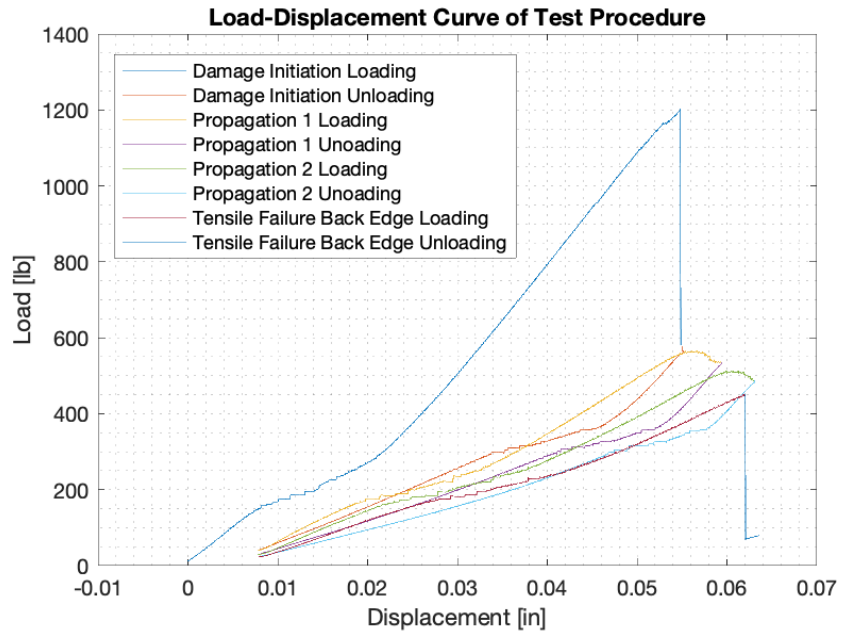
X-axis: Displacement [in]
Y-axis: Load [lb]

Figure 6. Load-displacement data of a typical test.

The matrix-compression strain-energy release rate was calculated using the Area Method (Corleto & Bradley, 1989; Hibbs, Ming, & Bradley, 1987). This method consists of loading the specimen to incipient propagation, unloading from this point, loading again, causing propagation to occur, and unloading again. The net energy associated with this load-unload cycle is assumed to be entirely associated with the propagation that occurred. Thus, accurate use of the Area Method requires that (1) specimens to be periodically loaded/unloaded, (2) minimal far-field damage occurs, and (3) the load and displacement returns consistently to the same values at each unload. Correspondingly in this study, requirement (1) was inherently met through the testing procedure, requirement (2) was met and verified through careful observation of the test specimens, and requirement (3) was observed to consistently be met as illustrated in Figure 7 where the shaded area corresponds to the energy associated with the propagation.
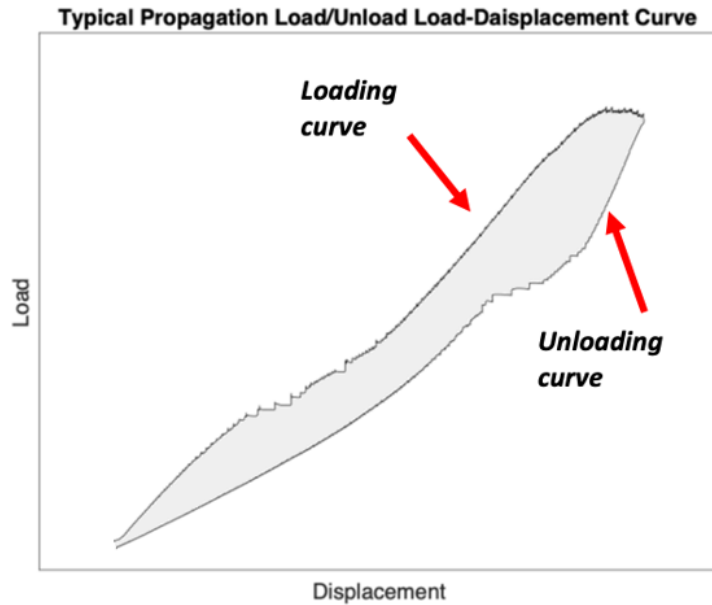
Figure 7. Loading and unloading data for a typical test.

Using the Area Method, the strain-energy release rate is calculated as:

$$G^{MC} = \frac{\Delta U}{B \Delta a} \tag{1}$$

Where G^{MC} is the calculated energy release rate, ΔU is the energy associated with the propagation, B is the fracture surface width, and Δa is the length of crack propagation. The parameter ΔU is the previously discussed area between the loading and unloading load

displacement curves. It was numerically calculated from the data collected during testing. The parameter B is the specimen through-thickness fracture path length. It is equal to the total length of the W-shaped through thickness transverse fracture path as viewed at the notch tip and as illustrated in Figure 8. It was calculated from images taken during testing using the MATLAB Image Viewer. Sectioning of specimens indicated that both the shape and size of this fracture path remained consistent throughout the fracture region of the specimen.
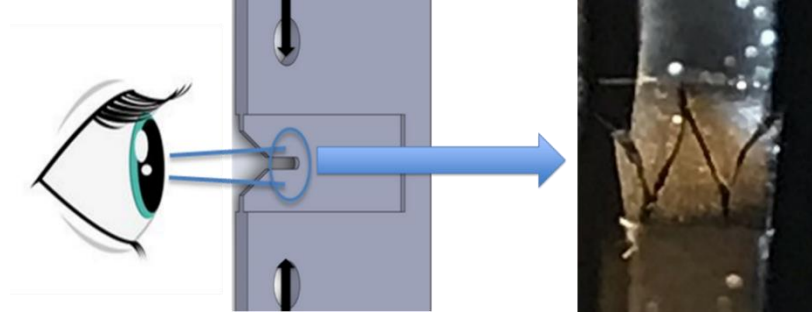

Figure 8. Specimen through-thickness fracture path.

The parameter Δa is the propagation distance. It is equal to the magnitude of the increase in the length of the notch tip crack due to the associated unload-reload cycle. It was calculated from images taken during testing using the MATLAB Image Viewer.

As calculated in Equation 1, G^{MC} is the total energy release rate. It is apparent from Figure 8 that the fracture path is oriented neither parallel nor perpendicular to the loading direction. Thus, the fracture that is occurring in mixed mode, a combination of Mode I and Mode II. Using fracture mechanics theory, the total matrix-compression strain energy is related to the Mode I and Mode II strain energies through the equation:

$$G_{Total}^{MC} = G_I^{MC} + G_{II}^{MC} \tag{2}$$

Where G_{Total}^{MC} is equal to G^{MC} from Equation 1, G_I^{MC} is the Mode I component of G_{Total}^{MC}, and G_{II}^{MC} is the Mode II component of G_{Total}^{MC}. The relative magnitudes of the two modal energy release rates are related through the Phase Angle ψ given by:

$$\psi = arctan \sqrt{\frac{G_{II}^{MC}}{G_I^{MC}}} \tag{3}$$

Combining Equation 2 and Equation 3 gives:

$$G_I^{MC} = G_{Total}^{MC} \left(\frac{1}{tan^2\psi}\right) \tag{4}$$

$$G_{II}^{MC} = G_{Total}^{MC} \left(\frac{tan^2\psi}{1 + tan^2\psi} \right) \tag{5}$$

Using the MATLAB Image Viewer, the Phase Angle was measured from images taken during testing. A single unique value of Phase Angle was calculated for each test specimen by (1) measuring the angle of inclination and the length of each of the four legs of the W-shaped fracture path (a typical path is shown in Figure 8) and (2) calculating an average of the four angles of inclination weighted by their respective lengths.

5   Results

Specimens tested were comprised of one of two materials. The first was a proprietary carbon fiber and epoxy, and the second was a commercially available carbon fiber and epoxy constructed of TR50S carbon fiber and NB301 epoxy. Manufacturing specimens according to the methods discussed in section 2 resulted in usable sample success rates of 88% and 63% for the proprietary and commercial material, respectively. Upon testing, it was discovered that the proprietary material specimens behaved as intended. However, none of the commercial material specimens behaved as intended. Specifically, loading the specimens to initial damage resulted in immediate damage propagation through the entire thin region, making propagation measurements impossible. The project concluded before remedial action was taken and revised commercial material specimens were manufactured and tested. As such, the remaining text in this section documents the results of the proprietary material only.

The resulting energy release rates and phase angle data from the 50 tests conducted are given in Table 1. Due to the non-disclosure requirements associated with the proprietary material, mean values and standard deviations of energy release rates measured in this project are given as multiples of the corresponding currently-used values. These values are reported with "units" of *cv. Mathematically:

$$mv = R * cv \tag{6}$$

where mv is the value measured in this project, R is a ratio calculated as the value measured in this project divided by the currently-used value, and cv is the currently-used value provided by the manufacturer of the proprietary carbon fiber material.

Table 1. Test results for the matrix-compression energy release rate.

Parameter	Symbol	Mean Value	Standard Deviation
Total Energy Release Rate	G_{Total}^{MC}	15.30 *cv	6.01 *cv
Mode I Energy Release Rate	G_I^{MC}	3.42 *cv	1.72 *cv
Mode II Energy Release Rate	G_{II}^{MC}	11.88 *cv	4.69 *cv
Phase Angle	ψ	62.14 degrees	4.16 degrees

Note: Test results for the matrix-compression energy release rate (the value currently used by the manufacturer is 1*cv). These ratios, when multiplied by the current value (*cv) of matrix-compression energy release rate used by the manufacturer, give the value measured in this study.

As a validation of the test specimen and test approach used in this study, the matrix-tension energy release rate was determined. This validation consisted of the same specimen, materials, test equipment, and analysis methods as used for the matrix-compression testing and analysis of this project except that the loading was tensile instead of compressive. A total of 12 specimens were tested. The result was a mean value of the matrix-tension energy release rate of 1.16 *cv with a standard deviation of 0.39 *cv. The manufacturer provided value of the matrix-tension energy release rate is 1*cv. This value falls well within the experimental uncertainty of the experimental measurement and the method is considered validated.

6   Finite element analysis

6.1   The matrix-compression material model

In evaluating a compressive crack or damage propagation material model a key consideration is the ability of the material behind the advancing crack or damage to carry load. This load-carrying ability arises since the material behind the advancing crack or region-of-damage remains in contact and has a reduced capability to support load. In the discussion that follows the term *tip* is used for the leading edge of the crack or region-of-damage and the term *wake* is used for the material behind this leading edge through which the crack or damage has passed, while retaining a reduced capability to support load. Overall, the energy release rate of the propagating crack can be partitioned into a contribution from the tip and a contribution from the wake.

$$G_{Total} = G_{Tip} + G_{Wake} \tag{7}$$

Where G$_{Total}$ is the previously defined G_{Total}^{MC}, G$_{Tip}$ is the energy release rate associated with propagation at the tip, and G$_{Wake}$ is energy release rate associated with any subsequent additional fracture occurring in the wake.

Figure 9 illustrates the tip and wake for the Compact Compression Specimen used in this study. The tip is located at the edge of the region-of-damage furthest from the notch. The wake extends from the tip to the notch. The tip is the observed propagating leading edge of matrix-compression fracture damage. The wake is the region in which matrix-compression fracture occurred but load-carrying ability remains.
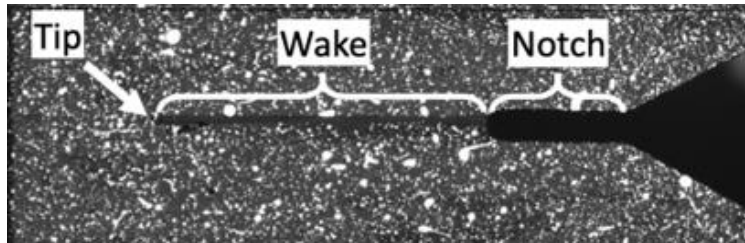

Figure 9. Magnified view of a fractured compact compression specimen identifying the tip, wake, and notch.

In Figure 9, the wake consists of a W-shaped fracture path. Closer examination reveals that at the vertices of this fracture path, ply delamination occurs as illustrated in Figure 10. Sectioning of several specimens indicates that this delamination consistently occurs throughout the wake.
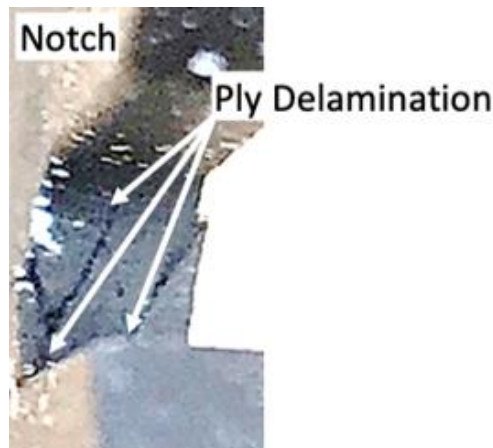

Figure 10. Magnified view of a fractured Compact Compression Specimen showing the ply delamination occurring in the wake.

Using these observations coupled with calculations the overall fracture behavior of the test specimen can be deduced. Damage initiates as a mixed mode fracture forming a W-shaped fracture path. This morphology is created consistently at the tip. Damage propagates in the wake as ply delamination at the vertices of the W-shaped fracture path. The values given in Table 1 combine the fracture occurring at the tip and in the wake. However, from private communication

with the manufacturer of the proprietary carbon fiber, a value of 0.261*cv was provided for the Mode I ply delamination. Using this value with crosshead displacement data as an estimate of delamination crack-propagation distance and crack length measurements as an estimate of delamination crack width, an approximate value of the energy associated with this crack propagation was calculated for all test specimens. This value was compared to the total energy of fracture (the ΔU parameter calculated from the area between the unloading and loading curves as illustrated in Figure 3) and found to be relatively very small. Numerically for all specimens tested this wake energy never exceeded 2.5% of the total energy and had an average value of 0.82% with standard deviation of 0.39%. Translating these results to the strain-energy release rates given in Equation 7, it is concluded that a good approximation G_{Total} can be assumed equal to G_{Tip}. The implications of this conclusion are significant. In subsequent simulations, the values given in Table 1 can be substituted for the currently used values for matrix-compression behavior. There is no need for special consideration for the inclusion of a wake effect.

6.2   The most effective means of ABAQUS implementation

Prior to beginning this project, it was expected that implementing the to-be-determined matrix-compression material model in ABAQUS would be rather complicated. This was because the overall energy release rate was expected to be a function of the amount of damage propagation. Specifically, that the contribution of G_{Wake} would be significant and would increase as the length of the wake increased. This would require ABAQUS programmatically tracking the length of the wake and updating the value of G_{Total} used in the simulations. Early in the project an ABAQUS VUMAT code was created with the intent to modify it as needed to implement the length tracking and updating of the value of G_{Wake} and G_{Total}. The discovery of that G_{Wake} was not significant greatly simplified implementation and allowed a simple substitution of the constant value of G_{Total} for the currently used value.

6.3   Implementation of the model in ABAQUS

The material model was implemented in two types of geometries. The first geometry is the test specimen geometry as illustrated in Figure 2. Due to the varying thickness of this geometry, implementation was done using an ABAQUS VUMAT code supporting 3D Hashin-Rotem damage initiation and propagation criteria that was created based on content from Wang, Pineda, Ranatunga & Smeltzer (2015). The required material properties for this VUMAT include a Mode-II matrix energy release rate and a total matrix-compression energy release rate (a Mode-I matrix energy release rate is not required as an input). These were given values of the measured Mode-II matrix-compression energy release rate (11.88*cv) and the measured total matrix-

15

compression energy release rate (15.30*cv) respectively given in Table 1. Other material properties required by the VUMAT were assigned currently used values by the manufacturer for the proprietary carbon fiber. Although not a significant contributor to the strain-energy release rate, the deformation and damage that occurred in the wake was significant in affecting the predicted load-displacement response of the specimen in the ABAQUS simulations. Initially the element-deletion feature of ABAQUS was used but this provided too extreme of a response and reduced load-carrying ability too much. An effective solution was found to be the "Smoothed Hydrodynamic Particles" (SPH) technique (Aktay, Johnson, & Kroplin, 2008; Aktay, Johnson, & Kroplin, 2005; Giannaros, Kotzakolios, & Kostopoulos, 2019). Often used with fluids, it can maintain load-carrying ability under large deformations. It is available in ABAQUS and was used for all simulations of the test specimen. The second implementation geometry is notched constant-thickness panels. This type of geometry was the subject of the prior AMTAS project at OSU entitled "Failure of Notched Laminates Under Out-of-Plane Bending." Implementation in this geometry type was done by using the same ABAQUS analysis used in the original AMTAS studies and simply substituting the "Total Energy Release Rate" of 15.30*cv given in Table 1 for the currently used value of 1*cv.

6.4   Verification simulations in ABAQUS

Verification was performed by comparing the load-displacement behavior of the test specimen as predicted by the ABAQUS simulations using the VUMAT described above to that measured in the experiments. The results of this comparison are illustrated in Figure 11. The blue, upper, curve with shaded region corresponds to the experimental results. The solid blue line is the mean value of the experimental results, and the shaded blue region is a 95% confidence interval. The red, middle, line corresponds to ABAQUS results using the experimentally measured values (Table 1) of 11.88*cv for the Mode-II matrix-compression energy release rate and 15.30*cv for the total matrix-compression energy release. The green, bottom, curve corresponds to ABAQUS results using the manufacturers currently used values of 1*cv for the Mode-II matrix-compression energy release rate and 1*cv for the total matrix-compression energy release. As shown, use of the experimentally measured values more strongly agrees with the experimental results than the currently used manufacturer values. Additional simulations showed that much closer agreement is possible by increasing the values of the currently used manufacturer Hashin-Rotem parameters of matrix strength (Yc) and transverse shear strength (St). Discussions with the manufacturer's technical personnel indicated such increase might be justified due to uncertainty in the values of these parameters. Given the approximate agreement shown in Figure

11 and the possibility of improving it through "tuning" of the two strength parameters, the material model is taken to be validated.
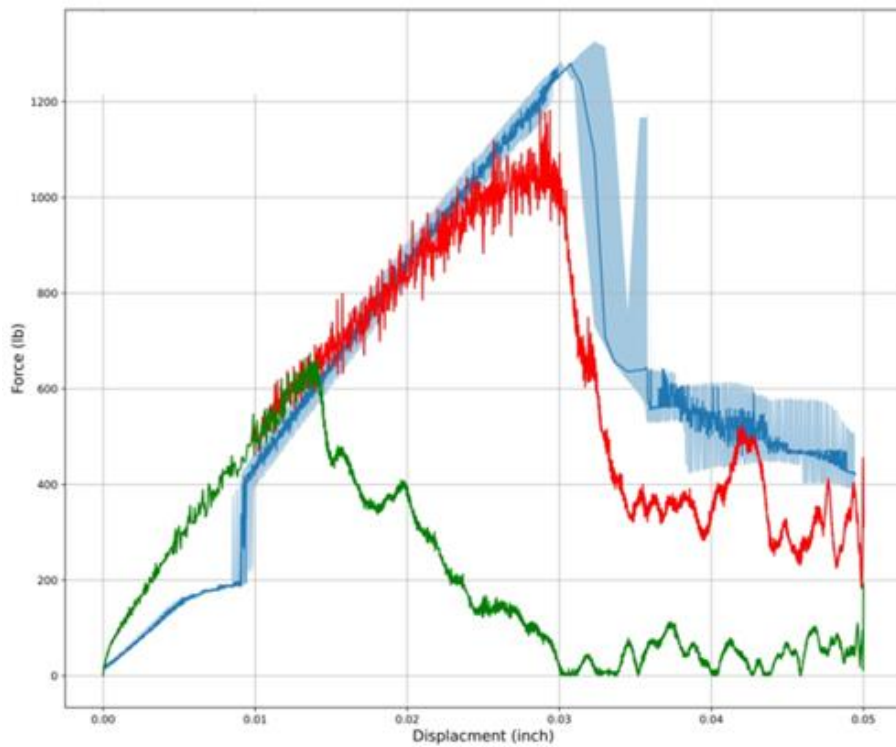

Figure 11. Comparison of load-displacement behavior as experimentally measured (blue) and as numerically calculated using the energy release rate currently used by the manufacturer (green) and that as determined in this study (red).

6.5   The extent to which the differences in damage models is significant.

The purpose of this subsection is to explore the effects of changing from the currently used value of the matrix-compression energy release rate to the value determined in this study for structural laminates potentially used in fuselage, wing, or empennage skins. This was pursued by selecting relevant laminate plate geometries and layups, implementing both the currently used value of the matrix-compression energy release rate and the value determined in this study, and comparing the resulting effect on a few relevant parameters.

6.5.1 Out-of-plane shear

Out-of-plane shear (i.e., Mode III loading) of an edge notched panel was selected for this task based on the extensive prior work performed through this AMTAS project entitled "Failure of Notched Laminates Under Out-of-Plane Bending." Figure 12 illustrates the associated geometry,

applied loading, undeformed mesh, and deformed mesh of the ABAQUS models. Details of the finite element modeling methods used has been published (Hyder, et al., 2016). Briefly, the models consist of 8 node, reduced integration continuum shell elements (ABAQUS SC8R) with a mesh density of 20 elements around the notch (element size of approximately 0.545 mm by 0.737 mm). Element size increased with increasing distance from the notch tip. Loading was displacement controlled.
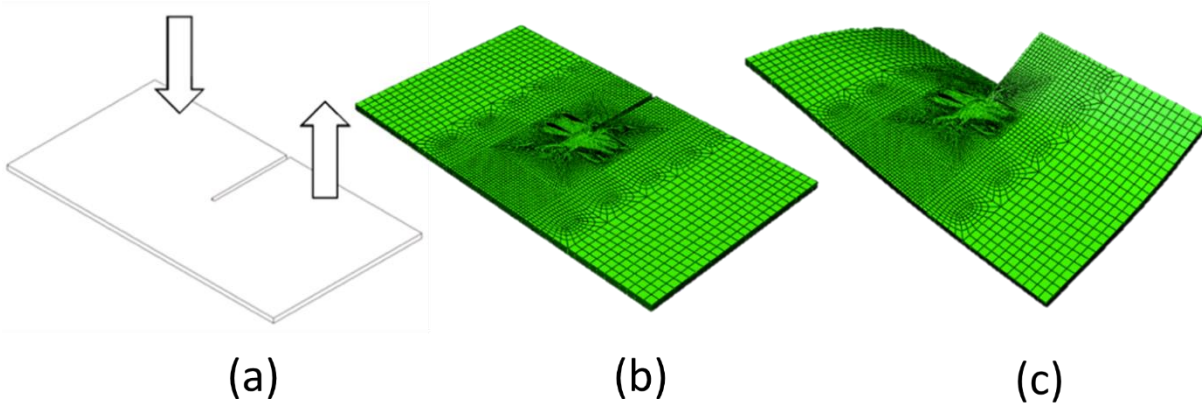

(a) (b) (c)

Figure 12. (a) Out-of-plane shear (Mode III) loading of an edge-notched plate showing (a) geometry and loading directions, (b) undeformed ABAQUS mesh, and (c) deformed ABAQUS mesh.

Through the AMTAS work, ABAQUS models were available for six proprietary laminated skin layups: A (40 plies, 10% zero-degree plies), B (40 plies, 30% zero-degree plies), C (40 plies, 50% zero-degree plies), D (20 plies, 10% zero-degree plies), E (20 plies, 30% zero-degree plies), and F (20 plies, 50% zero-degree plies).

For each layup, comparisons of Mises stress, fiber-tension damage, fiber-compression damage, matrix-tension damage, and matrix-compression damage were made using the currently used manufacturers value of 1*cv and the value determined in this study of 15.30*cv of the matrix-compression energy release rate. Loading was displacement controlled and held equal in all comparisons.

Typical results (layup D) are shown in Figure 13 for Mises stress. These results show that the change in the value of the energy release rate does not tend to change maximum stress magnitude greatly but does affect the stress distribution. Note in Figure 13 contour values are equal between plots where red is the greatest magnitude and darkest blue is the least magnitude.
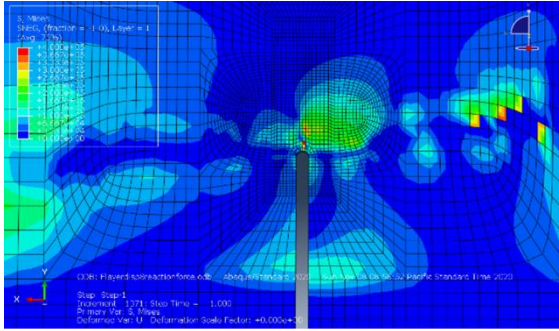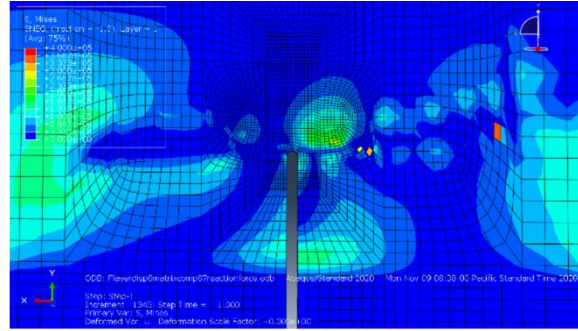
Figure 13. Typical out-of-plane shear Mises stress distributions for (a) Gmc = 1*cv and (b) Gmc = 15.30*cv (full-panel undeformed geometries).

As might be expected, the fiber-tension damage and fiber-compression damage were in general not significantly affected for any of the laminated skin layups by the change in energy release-rate value.

Also, as might be expected, the greater value of the matrix-compression energy release rate resulted in a decrease in matrix damage. Figure 14 shows a typical result (layup E). Note the contour values are equal between plots where red corresponds to a damage value of one (no load-carrying ability) and darkest blue to a damage value of zero (no damage).
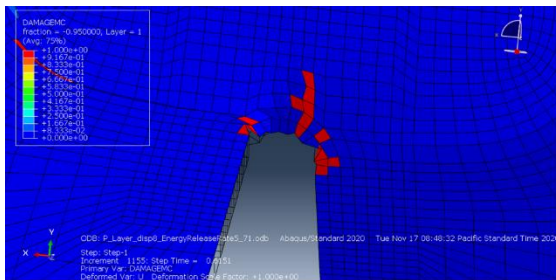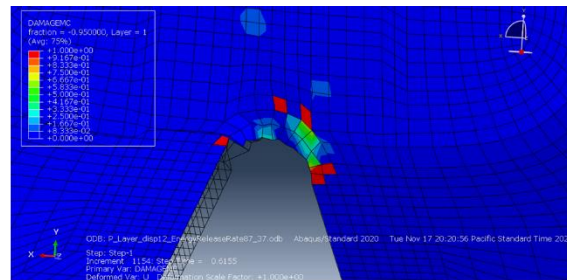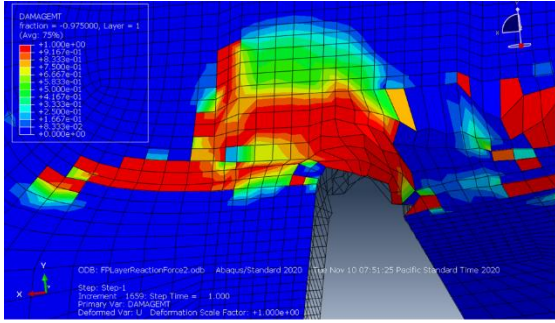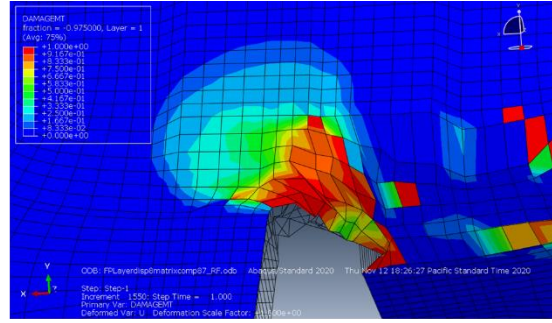

Figure 14. Typical matrix-compression damage distributions for (a) Gmc = 1*cv and (b) Gmc = 15.30*cv (notch-tip deformed geometries).

The most affected parameters were matrix-tension damage and shear damage, and typical results (layup A) are shown respectively in Figure 15 and Figure 16. In both cases distributions remained similar but magnitudes changed significantly. In both figures, contour values are equal between plots where red corresponds to a damage value of one (no load-carrying ability) and darkest blue to a damage value of zero (no damage).
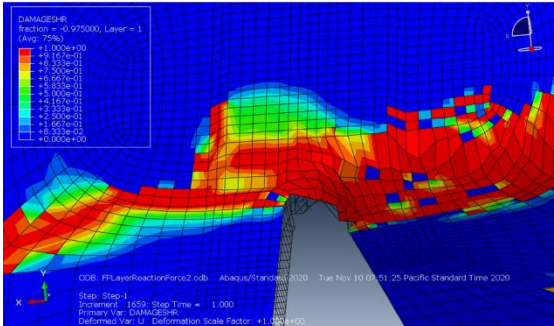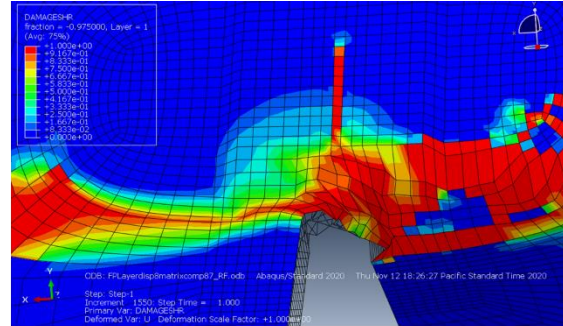
19

Figure 15. Typical matrix-tension damage distributions for (a) Gmc = 1*cv and (b) Gmc = 15.30*cv (notch-tip deformed geometries).

Figure 16. Typical shear damage distributions for (a) Gmc = 1*cv and (b) Gmc = 15.30*cv (notch-tip deformed geometries).

Given these results, predictions can be made regarding load-transfer mechanisms and structural residual strength. In regions of compression, the decrease in matrix-compression damage would tend to increase the load-carrying ability of the matrix, relieving load on stiffening elements (fibers), and increasing residual strength. In regions of tension or shear, the change in magnitude of damage will correspond to either transferring load to stiffening elements if damage increases, or relieving load from stiffening elements if damage decreases. Overall, load transfer from stiffening elements to the matrix will tend to increase the arresting of penetrating damage due to delamination growth.
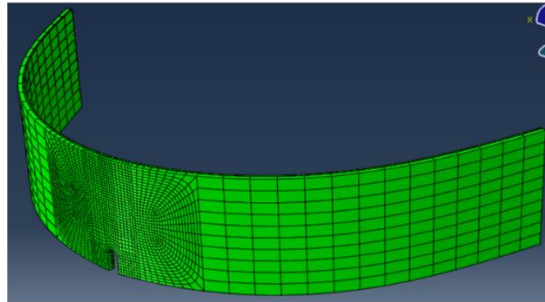
6.5.2 Out-of-plane bending

Out-of-plane bending of a center notched panel was also selected for this task based on the extensive prior work performed through the AMTAS project entitled *Failure of Notched Laminates Under Out-of-Plane Bending*. Figure 17 illustrates the associated geometry, applied loading, undeformed mesh, and deformed mesh of the ABAQUS models. Details of the associated finite element modeling are available in numerous presentations and prior reports (Parmigiani & Kennedy, 2010). Briefly, the models consist of 8 node, reduced integration continuum shell elements (ABAQUS SC8R) with a mesh density of 12 elements around the notch (element size of approximately 0.83 mm by 2.63 mm). Element size increased with increasing distance from the notch tip. Loading was displacement controlled. All results given are at the same value of displacement.
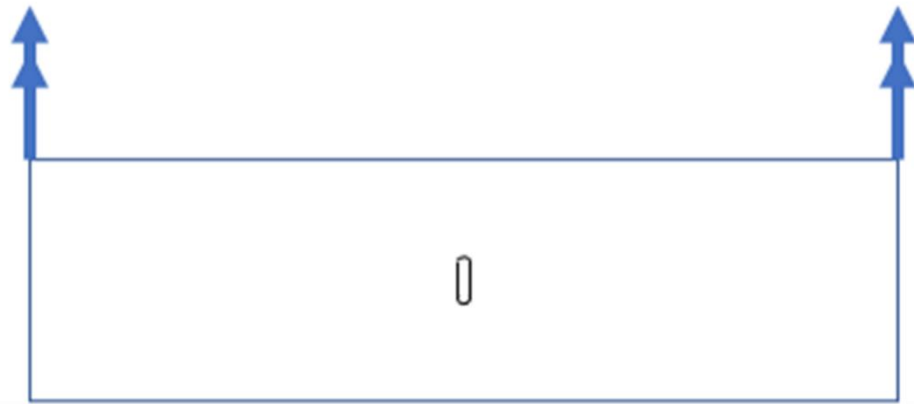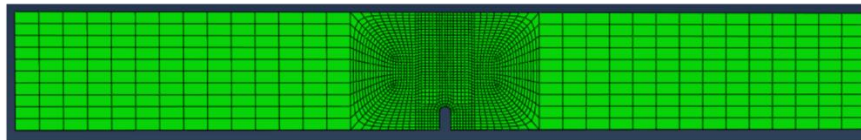
Figure 17. Out-of-plane bending loading of a center-notched plate showing (a) geometry and loading directions, (b) undeformed ABAQUS mesh (half model), and (c) deformed ABAQUS mesh (half model, deformation magnified).

Through the AMTAS work, ABAQUS models were available for six proprietary layups: A (40 plies, 10% zero-degree plies), B (40 plies, 30% zero-degree plies), C (40 plies, 50% zero-degree plies), D (20 plies, 10% zero-degree plies), E (20 plies, 30% zero-degree plies), and F (20 plies, 50% zero-degree plies).

Comparisons of Mises stress, fiber-tension damage, fiber-compression damage, matrix-tension damage, and matrix-compression damage were made using the currently used manufacturers value of 1*cv and the value determined in this study of 15.30*cv of the matrix-compression energy release rate. Loading was displacement controlled and held equal in all comparisons.

Results for Layup D are shown in Figure 18 through Figure 21. Overall, results for out-of-plane bending are consistent with those for out-of-plane shear.

Results as shown in Figure 18 indicate that the change in the value of the energy release rate does not tend to change maximum Mises stress magnitude greatly but does affect the stress distribution slightly. Note contour values are equal between plots where red is the greatest magnitude and darkest blue the least magnitude.
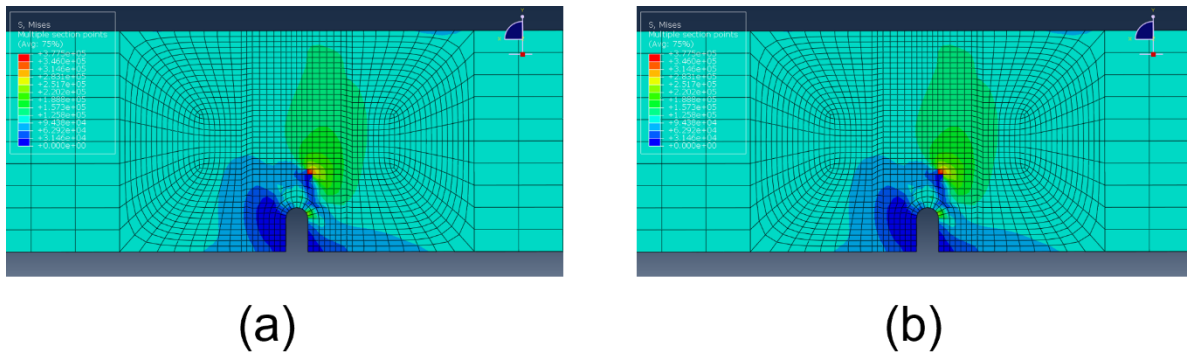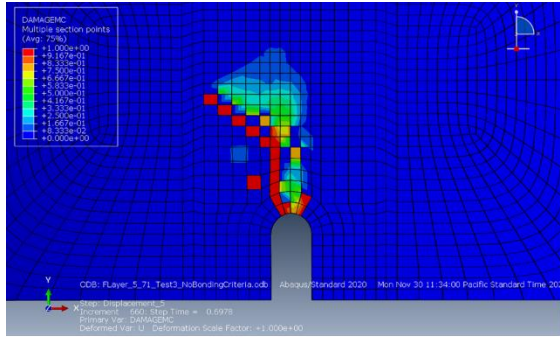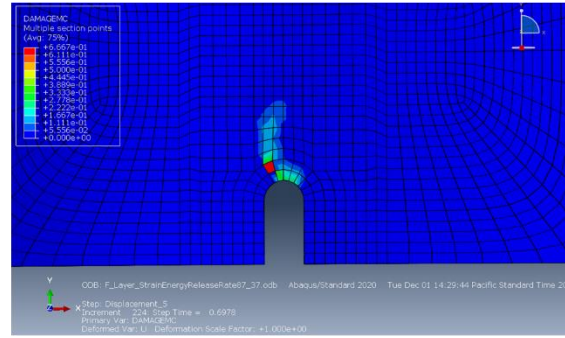

(a)   (b)

Figure 18. Proprietary layup D out-of-plane bending Mises stress distributions on tensile surface for (a) Gmc = 1*cv and (b) Gmc = 15.30*cv (full-panel undeformed geometries).

As was true for out-of-plane shear, the fiber-tension damage and fiber-compression damage were not significantly affected by the change in energy release rate value.

Figure 19 shows the damage plots for matrix compression on the compression surface of the panel for both energy release rates. Note in Figures 19 through 21, contour values are equal between plots where red corresponds to a damage value of one (no load-carrying ability) and darkest blue to a damage value of zero (no damage). The greater value leads to less damage as expected. This reduction in damage causes a redistribution of load. The lesser damaged matrix is capable of supporting additional load, relieving load from stiffening elements (fibers) increasing overall load-carrying ability. Penetrating damage might be more readily arrested due to delamination growth.
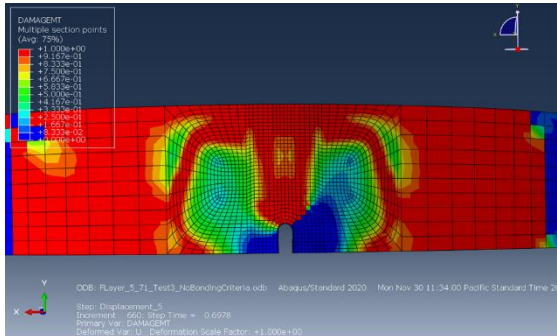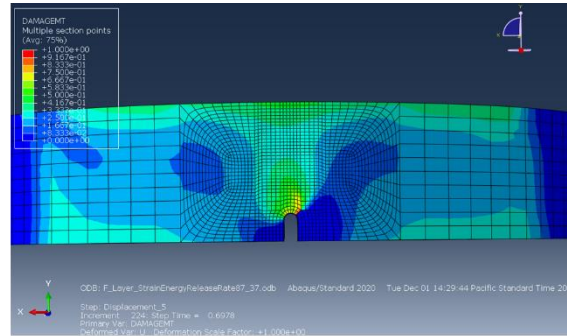
Figure 19. Proprietary Layup D out-of-plane bending matrix-compression damage distributions on compression surface for (a) Gmc = 1*cv and (b) Gmc = 15.30*cv (notch-tip deformed geometries).

As illustrated in Figure 20, the change in energy release rate leads to significant changes in the matrix-tension damage.

Figure 20. Proprietary Layup D matrix-tension damage distributions on tensile surface for (a) Gmc = 1*cv and (b) Gmc = 15.30*cv (notch-tip deformed geometries).

Figure 21 illustrates the change in energy release rate that also resulted in substantial changes in the shear damage presence and distribution.
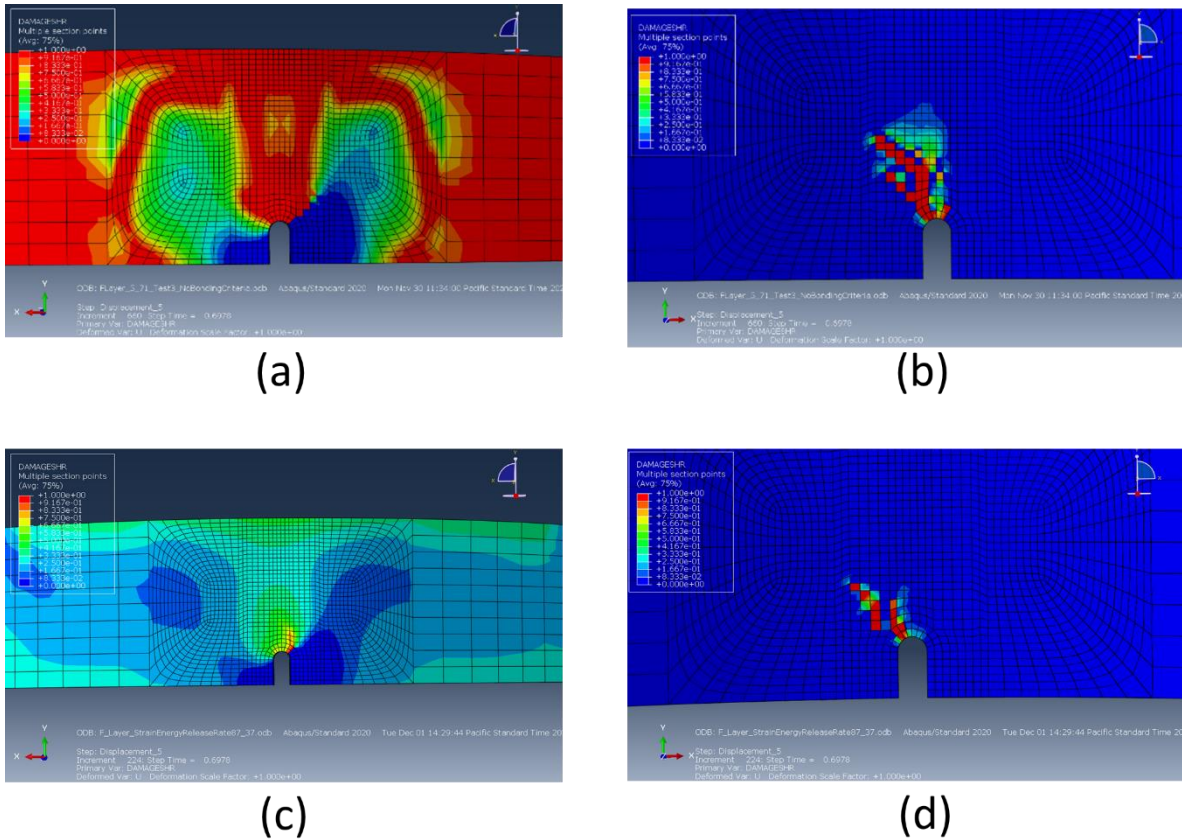
Figure 21. Proprietary Layup D shear damage distributions for compression surface (a) Gmc = 1*cv and (b) Gmc = 15.30*cv (notch-tip deformed geometries) and tensile surface (c) Gmc = 1*cv and (d) Gmc = 15.30*cv (notch-tip deformed geometries).

The above figures show significant decreases in matrix tension and shear damage. These decreases lead to the matrix carrying additional load and thus relieving load from stiffening elements (fibers) increasing overall load carrying ability. The mechanism of penetrating damage propagation is also affected possibly by increased tendency to arrest damage due to delamination in the matrix.

6.6   The effect of statistical variation

As shown in Table 1, the statistical variation in the experimentally measured values of the matrix-compression energy release rate was relatively large. The effect of this variation is illustrated by considering the out-of-plane shear of the proprietary A layup. Specifically, ABAQUS simulations were performed for this layup using a value of the matrix-compression energy release rate equal to the currently used value of 1 *cv, one standard deviation less than the mean of the Experimentally Measured value (9.29 *cv), the mean of the Experimentally Measured value of (15.30 *cv), and one standard deviation greater than the mean value (21.31

*cv). The results for Mises stress are illustrated in Figure 22. Note contour values are equal between plots red is the greatest magnitude and darkest blue the least magnitude.
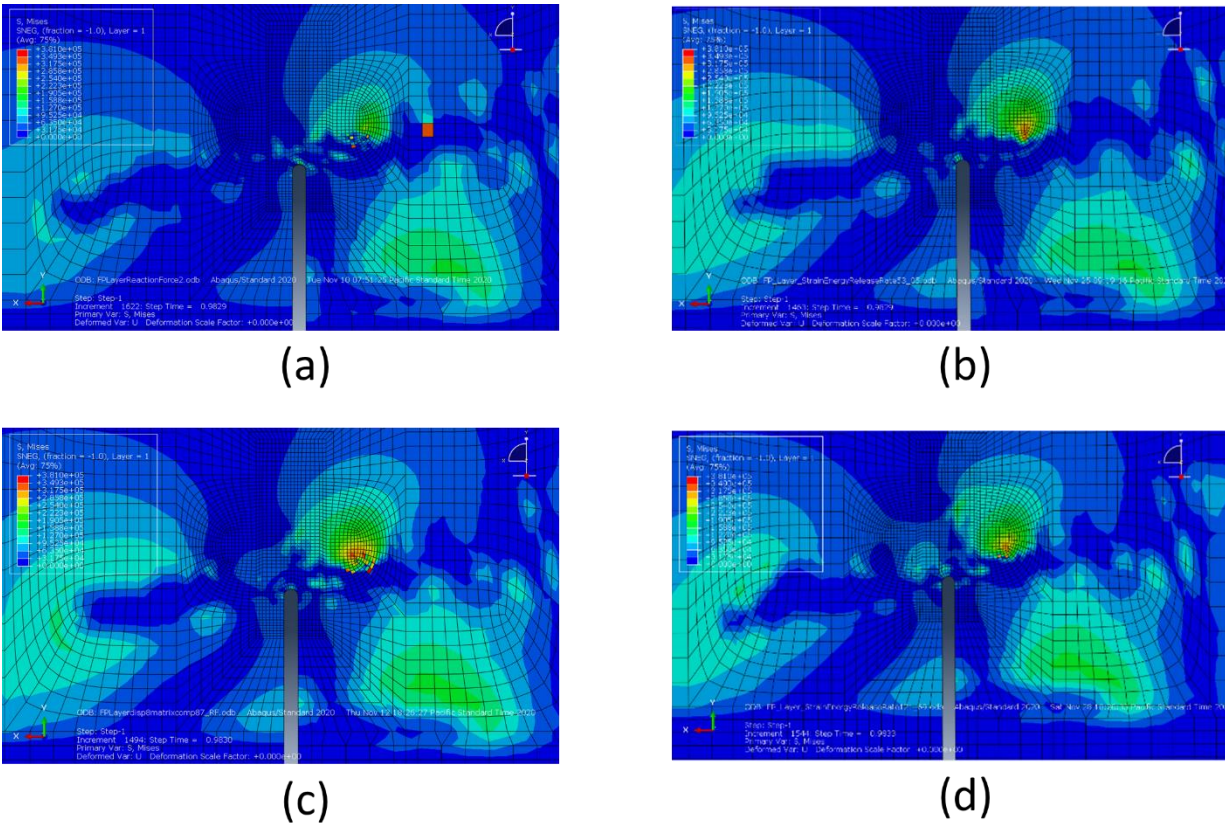

(a)

(b)

(c)

(d)

Figure 22. Out-of-plane shear Mises stress distributions for proprietary layup A (a) Gmc = 1*cv, (b) Gmc = 9.29*cv, (c) Gmc = 15.30*cv, and (d) Gmc = 21.31*cv (full-panel undeformed geometries).

As might be expected, the fiber-tension damage and fiber-compression damage were in general not significantly directly affected for any of the layups by the change in energy release rate value. If the same results were reviewed in stiffened structures including discrete longitudinal stringers and frames or ribs, changes in matrix and shear stresses would indirectly affect the load transfer of fiber stress concentrations to these stiffening elements, affecting overall local stability, fiber stresses and catastrophic propagation of the penetrating damage.

Results for matrix-compression damage are given below in Figure 23. Note contour values are equal between plots where red corresponds to a damage value of one (no load-carrying ability) and darkest blue to a damage value of zero (no damage).

Figure 23. Out-of-plane shear matrix-compression damage for proprietary layup A (a) Gmc = 1*cv, (b) Gmc = 9.29*cv, (c) Gmc = 15.30*cv, and (d) Gmc = 21.31*cv (notch-tip deformed geometries).

Results for matrix-tension damage and shear damage are given in Figure 24 and Figure 25, respectively. In both figures, contour values are equal between plots where red corresponds to a damage value of one (no load-carrying ability) and darkest blue to a damage value of zero (no damage).
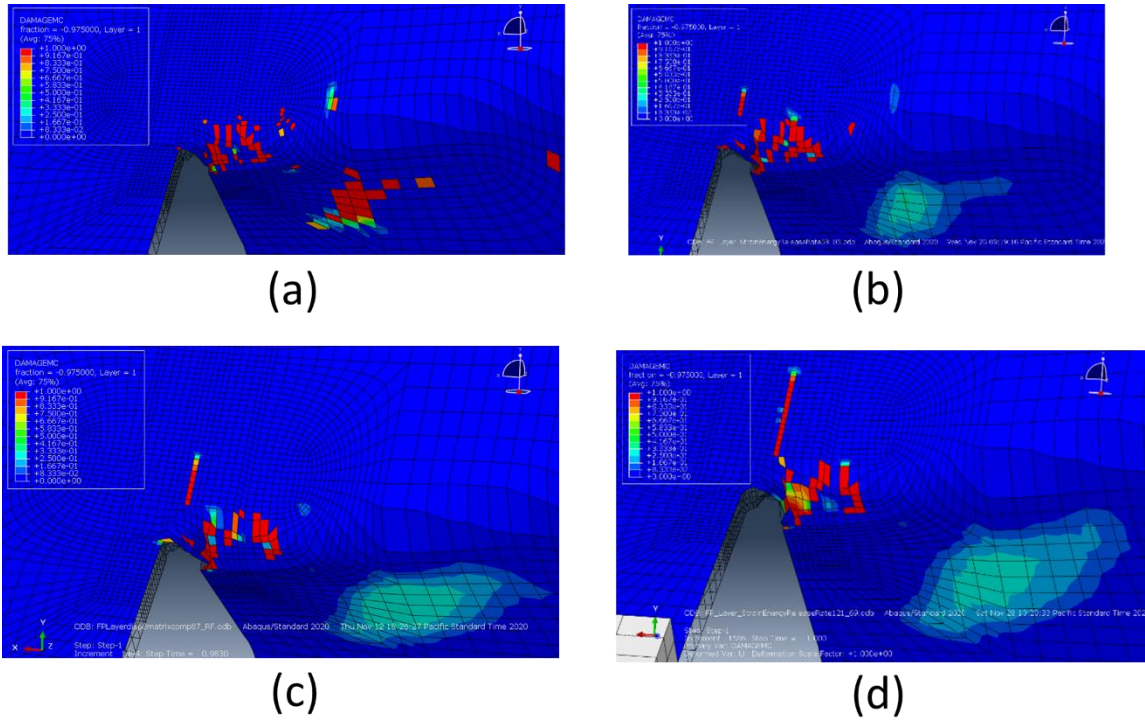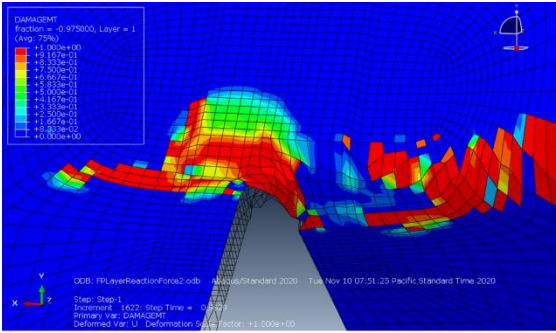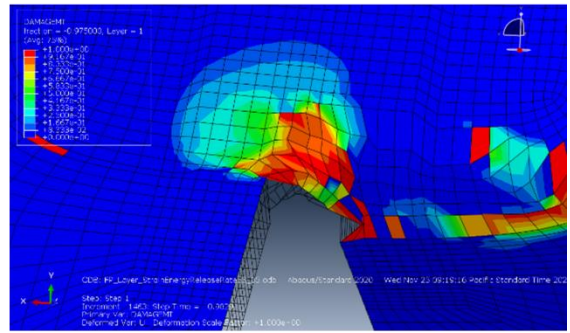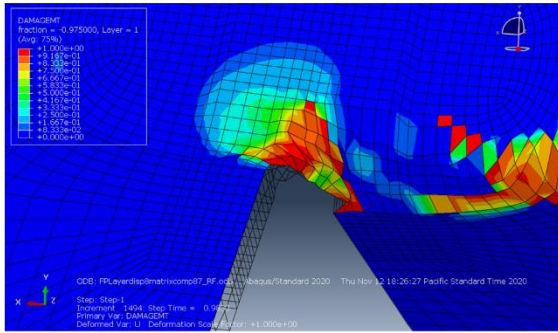
Figure 24. Out-of-plane shear matrix-tension damage for proprietary layup A (a) Gmc = 1*cv, (b) Gmc = 9.29*cv, (c) Gmc = 15.30*cv, and (d) Gmc = 21.31*cv (notch-tip deformed geometries).
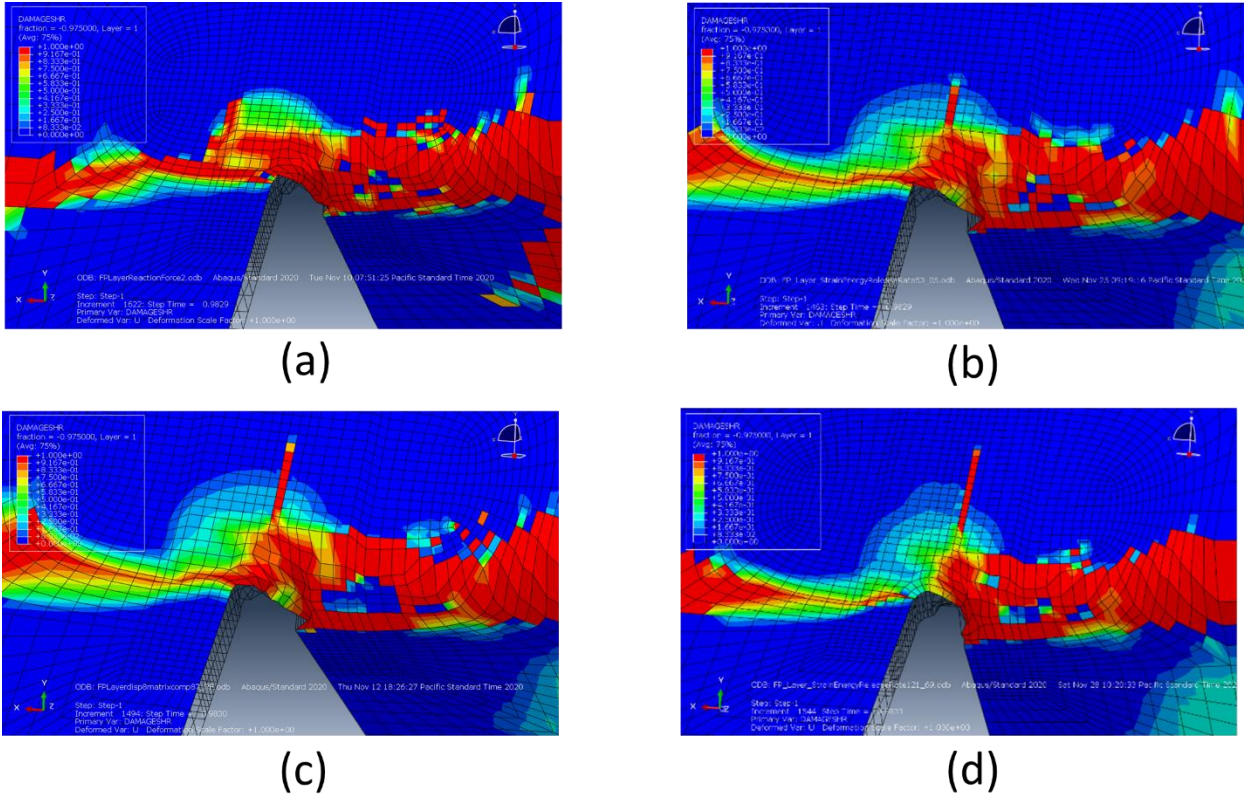
Figure 25. Out-of-plane shear damage for proprietary layup A (a) Gmc = 1*cv, (b) Gmc = 9.29*cv, (c) Gmc = 15.30*cv, and (d) Gmc = 21.31*cv (notch-tip deformed geometries).
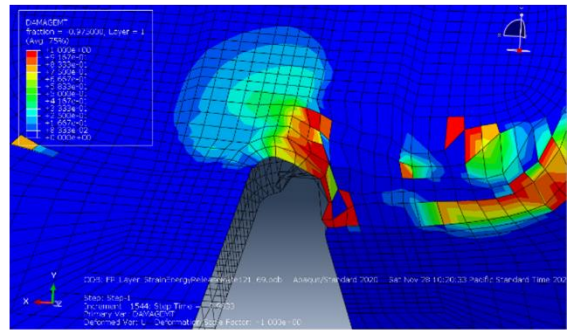
7   Conclusions

The goals of this project were to experimentally determine a new physically realistic material model for matrix-compression and then to implement this model into ABAQUS and evaluate its effects. These goals were achieved. Specifically, a test specimen and associated test and analysis procedures were defined, a physically realistic material model was determined, the model parameters were measured, a means of implementation was identified, implementation was performed in ABAQUS, the ABAQUS simulation was validated, and the effects of the new material model on ABAQUS predictions were shown. Experimental observations allowed the decomposition of the energy release rate into its Mode I and Mode II components. A significant finding is that, at least under the conditions of this study, the matrix-compression energy release rate, to a good approximation, is not a function of the amount of matrix-compression damage created (i.e., G_{mc} is not a function of the length of the crack wake). This finding allows the value of G_{mc} determined through this study to be implemented in simulations as a simple direct

substitution of the currently used value. Implementation into geometries and layups of prior AMTAS projects showed that changing from the currently used value to the value determined in this study resulted in significant changes in component load-carrying ability. Overall, this report shows that the current method of simply using a tensile value for matrix-compression damage can introduce significant errors in predictions of damage initiation and propagation in finite element simulations of carbon-fiber laminates, characteristic of the skin in critical wing, fuselage, and empennage structures.

Based on these results it is recommended that the use of tensile damage behavior to estimate compressive damage behavior should cease. Proper testing should be conducted to determine compressive damage behavior directly since a tensile estimate has proven to be inaccurate. Any future work should include testing of commercially available material, a step unable to be completed prior to this project's conclusion. This testing will further support the projects findings. This is necessary, particularly in real structural configurations where the matrix and shear damage modes indirectly affect fiber load redistribution into any bonded or co-cured longitudinal stiffening elements and transverse framing or stiffening elements (e.g., wing and empennage ribs).

8   References

Aktay, L., Johnson, A., & Kroplin, B.-H. (2005). Semi-adaptive coupling technique for the prediction of impact damage. *VIII International Conference on Computational Plasticity.* Barcelona.

Aktay, L., Johnson, A., & Kroplin, B.-H. (2008). Numerical modeling of honeycomb core crush behavior. *Engineering Fracture Mechanics*(75(9)), 2616-2630.

Argon, A. (1972). Fracture of composites. *Treatise on Material Science and Technology, Vol. 1*, 79-114. doi:https://doi.org/10.1016/B978-0-12-341801-2.50007-2

Bazant, Z. O., & Oh, B. (1983). Crack band theory for the fracture of concrete. *Materials and Structures, Vol. 16*, pp. 155-177.

Budiansky, B. (1983). Micromechanics. *Computers and Structures, vol. 16*, pp. 3-12.

Corleto, C., & Bradley, W. (1989). Mode II delamination fracture toughness of unidirectional graphite/epoxy composites. In *Composite Materials: Fatigue and Fracture* (Vol. Second, pp. 201–221). West Conshohocken, PA: ASTM International.

Daniels, M. A., Rawlings, T. J., & Parmigiani, J. P. (2017). Experimental specimen selection for stress-displacement behavior and crack initiation in fiber reinforced composites. *Proceedings of the ASME 2017 International Mechanical Engineering Congress and Exposition. Volume 1: Advances in Aerospace Technology.* Tampa: ASME. doi:https://doi.org/10.1115/IMECE2017-71127

Daniels, M., & Rawlings, T. P. (2016). Selection and validation of experimental specimens for determining model inputs for matrix compression damage propagation in fiber reinforced composites. *Proceedings of the ASME 2016 International Mechanical Engineering Congress and Exposition. Volume 1: Advances in Aerospace Technology.* Phoenix: ASME. doi:https://doi.org/10.1115/IMECE2016-65682

Davila, C. G., Camanho, P. P., & Rose, C. A. (2005). Failure criteria for FRP laminates. *Journal of Composite Materials, vol. 39*(no. 4).

Fleck, N., Jelf, P., & Curtis, P. (1995). Compressive Failure of Laminated and Woven Composited. *Journal of Composites Technology and Research, vol. 17, no. 3*, pp. 212-220.

Gay, D. (2014). *Composite materials design and application* (3rd ed.). CRC Press.

Giannaros, E., Kotzakolios, A., & Kostopoulos, V. (2019). Hypervelocity impact response of CFRP laminates using smoothed particle hydrodynamics method: Implementation and validation. *International Journal of Impact Engineering, 123*, 56-69. doi:https://doi.org/10.1016/j.ijimpeng.2018.09.016

Gonzalez, C., & Llorca, J. (2007). Mechanical behavior of unidirectional fiber-reinforced polymers under transverse compression: Microscopic mechanisms and modeling. *Composites Science and Technology, Vol. 67*(No 13), pp. 2795–2806. doi:https://doi.org/10.1016/j.compscitech.2007.02.001

Gutkin, R., Laffan, M. L., Pinho, S. T., Robinson, P., & Curtis, P. T. (2011). Modelling the R-curve effect and its specimen dependence. *International Journal of Solids and Structure, vol. 48*, pp. 1767-1777.

Gutkin, R., Pinho , S., Robinson, P., & Curtis, P. (2010). On the transition from shear-driven fibre compressive failure to fibre kinking in notched CFRP laminates under longitudinal compression. *Composites Science and Technology, vol. 70*, pp. 1223-1231. doi:ttps://doi.org/10.1016/j.compscitech.2010.03.010

Han, Y., Hahn, H., & Croman, R. (1988). A simplified analysis of transverse ply cracking in cross-ply. *Composites science and Technology, vol. 31* , pp. 165-177.

Hibbs, M. F., Ming, K. T., & Bradley, W. L. (1987). Interlaminar fracture toughness and real-time fracture mechanism of some toughened graphite/epoxy composites. In *ASTM Special Technical Publication* (pp. 115–130). ASTM International.

Hyder, I., Froemming, T., Daniels, M., Beattie, W., Bay, B., & Parmigiani, J. (2016). Mode III loading of composite panels. *Journal of Aircraft, 53(2)*, 343-350.

Jelf, P. M., & Fleck, N. A. (1992). Compression failure mechanisms in unidirectional composites. *Journal of Composite Materials, vol. 26*, pp. 2706-2728.

Jose, S., Kumar, R., Jana, M., & Rao, G. (2001). Intralaminar fracture toughness of a cross-ply laminate and its constituent sub-laminates. *Composites Science and Technology, Vol. 61*(8), 1115-1122. doi:https://doi.org/10.1016/S0266-3538(01)00011-2

Kongshavn, I., & Poursartip, A. (1999). Experimental investigation of strain-softening approach to predicting failure in notched fibre-reinforced composite laminates. *Composites Science and Technology, vol. 59*(1), pp. 29-40.

Laffan, M., Pinho, S., Robinson, P., & Iannucci, L. (2010). Measurement of the in situ ply fracture toughness associated with mode I fibre tensile fracture in FRP. Part II: size and layup effects. *Composites Science and Technology, vol. 70*, pp. 614-621.

Laffan, M., Pinho, S., Robinson, P., & McMillan, A. (2011). Translaminar fracture toughness: The critical notch tip radius of 0 degree plies in CFRP. *Composites Science and Technology, Vol. 72*, pp. 97-102.

Lapczyk, & Hurtado, J. (2007). Progressive damage modeling in fiber-reinforced materials. *Composites Part A: Applied Science and Manufacturing, Vol. 38*, pp. 2333-2341.

Lu, M. L., Lee, C.-B., & Chang, F.-C. (1995). Fracture toughness of ABS by J-Integral methods. *Polymer Engineering and Science, vol. 35* (no. 18).

Maimi, P., Camanho, P., Mayugo, J., & Davila, C. (2007). A continuum model for composite laminates: Part I-constituitive model. *Mechanics of Materials, vol. 39* , pp. 897-908.

Maimi, P., Camanho, P., Mayugo, J., & Turon, A. (2011). Matrix cracking and delamination in laminated composites. Part I: Ply constitutive law, first ply failure and onset of delamination. *Mechanics of Materials, 43*(4), 169-185. doi:https://doi.org/10.1016/j.mechmat.2010.12.003

McKinley, T. A., Carpenter, K. T., & Parmigiani, J. P. (2018). *Development of novel compact compression specimen for matrix compression damage initiation and propagation behavior in fiber reinforced composites* (Vols. 9: Mechanics of Solids, Structures, and Fluids). American Society of Mechanical Engineers.

Narayanan, S., & Schadler, L. (1999). Mechanisms of kink-band formation in graphite/epoxy composites: a micromechanical experimental study. *Composites Science and Technology, Vol. 59*(No. 15), p.p. 2201–2213.

Parmigiani, J., & Kennedy, T. (2010). Failure of notched laminates under out-of-plane bending. *Sixth Annual Technical Review Meeting.* Seattle: FAA Joint Advanced Materials and Structures (JAMS) Center of Excellence.

Pinho, S. T., Gutkin, R., Pimenta, S., De Carvalho, N. V., & Robinson, P. (2012). On longitudinal compressive failure of carbon-fibre-reinforced polymer: from unidirectional to woven, and from virgin to recycled. *Phil. Trans. R. Soc. A, 370*, pp. 1871-1895. doi:https://doi.org/10.1098/rsta.2011.0429

Pinho, S., Robinson, P., & Lannucci, L. (2006). Fracture toughness of the tensile and compressive fibre failure modes in laminated composites. *Composites Science and Technology, vol. 66*, pp. 2069-2079.

Puck, A., & Schurmann, H. (1998). Failure analysis of FRP Laminates by means of physically based phenomenlogical models. *Composites Science and Technology, Vol. 58*, pp. 1045-1067.

Rawlings, T. J., Carpenter, K. T., & Parmigiani, J. P. (2018). Experimental specimen for classification of matrix compression damage in carbon fiber reinforced polymers. *American Society of Mechanical Engineers*, *vol. 1*: Advances in Aerospace Technology.

Soutis, C., & Curtis, P. (2000). A method for predicting the fracture toughness of CFRP laminates failing by fibre microbuckling. *Composites Part A: Applied Science and Manufacturing, Vol. 31*(No. 7), pp. 733-740.

Sutcliffe, M., & Fleck, N. (1994). Mirobuckle propagation in fibre composites. *Acta Mateallurgica et Materilia, Vol. 42*, pp. 2219-2231.

Toygar, M. E., Toparly, M., & Uyulgan, B. (2006.). An investigation of fracture toughness of carbon/epoxy composites. *Journal of Reiforced Plasticas and Composites, vol. 25,* (no. 18), pp. 1887-1895.

Vinod, M., B.J, S., N. V., Raghavendra, S., Murali, M., & Nafidi, A. (2010). Fractography of compression failed carbon fiber. *Journal of Mechanical Engineering Research, vol. 2 ,* pp. 001-009.

Wang, J., Pineda, E., Ranatunga, V., & Smeltzer, S. (2015). 3D progressive damage modeling for laminated composite based on crack band theory and continuum damage mechanics. *Annual Technical Conference of the American Society for Composites.* East Lansing, MI.